

Computer-based tracking of single sperm

Linda Z. Shi

University of California, San Diego
Department of Bioengineering
9500 Gilman Drive
La Jolla, California 92093

Jaclyn M. Nascimento

University of California, San Diego
Department of Electrical and
Computer Engineering
9500 Gilman Drive
La Jolla, California 92093

Michael W. Berns

University of California, San Diego
Department of Bioengineering
9500 Gilman Drive
La Jolla, California 92093
and
University of California, Irvine
Beckman Laser Institute
Department of Biomedical Engineering
1002 Health Sciences Road East
Irvine, California 92612

Elliot L. Botvinick

University of California, Irvine
Beckman Laser Institute
Department of Biomedical Engineering
1002 Health Sciences Road East
Irvine, California, 92612

1 Introduction

The measurement of sperm motility has been a major focus of basic and clinical sperm research for over 25 years. In fertility studies, the 1 to 5 (slowest-to-fastest) speed of progression (SOP) score is often used to characterize overall motility of a semen sample and to assess sperm quality.¹ This kind of scoring system is subjective and can be replaced by a quantitative measure based on objective computer scoring system.

Computer-assisted sperm analysis (CASA) systems have been commercially available since the mid-1980s. The goal of CASA systems has been to obtain objective data on sperm motility that can be used in research, human fertility clinics, and animal breeding programs. A detailed review of CASA can be found in Amann et al. (2004)² and Mortimer (1994).³ Widely used commercial CASA systems include the HTM-IVOS (Hamilton-Thorne Bioscience, Beverly, Massachusetts), the SM-CMA system (Stromberg-Mika, Bad Feilnbach, Germany), and the Hobson Sperm Tracker (Hobson Sperm Tracking Ltd, Sheffield, United Kingdom). There are also several noncommercial laboratory CASA systems.⁴⁻⁷ The percentage of motile sperm and velocity parameters such as

Abstract. This paper describes a robust single sperm tracking algorithm (SSTA) that can be used in laser optical trapping and sperm motility studies. The algorithm creates a region of interest (ROI) centered about a sperm selected by the user. SSTA contrast enhances the ROI image and implements a modified four-class thresholding method to extract the tracked sperm as it transitions in and out of focus. The nearest neighbor method is complemented with a speed-check feature to aid tracking in the presence of additional sperm or other particles. SSTA has a collision-detection feature for real or perceived collision or near-miss cases between two sperm. Subsequent postcollision analysis employs three criteria to distinguish the tracked sperm in the image. The efficacy of SSTA is validated through examples and comparisons to commercially available computer-aided sperm tracking systems. © 2006 Society of Photo-Optical Instrumentation Engineers. [DOI: 10.1117/1.2357735]

Keywords: sperm; tracking; motility; automation; CASA.

Paper 05387R received Dec. 22, 2005; revised manuscript received May 1, 2006; accepted for publication Jun. 30, 2006; published online Oct. 3, 2006.

swimming speed (curvilinear velocity), average path velocity, and straight line swimming speed are determined by these systems.

The CASA systems differ in their grayscale bit-depth, search region for finding the sperm in the next frame, frame rate, number of consecutive frames analyzed, grayscale thresholding method, image segmentation method to determine the pixel coordinates of the sperm, head versus mid-piece tracking, strategies for handling collisions and/or near-miss cases with other bright particles or sperm, and loss of focus during tracking.

Optical tweezers to measure sperm swimming force and swimming properties is a very different method to study sperm motility.⁸ Effects of optical trapping on sperm motility were first described by Tadir et al. (1989).⁹ The measurement and calculation of laser trapping forces on human sperm was described by Konig et al. (1996)¹⁰ and the effect of cryo-preservation on the relative laser trapping escape force was reported by Dantas et al. (1995).¹¹ The correlation between sperm swimming forces, their swimming speed, and the SOP score was recently reported by Nascimento et al. (2006).¹²

Thus far, sperm trapping experiments involve single sperm studies and require manually driven video analysis in a frame-by-frame manner to measure swimming velocities prior to and

Address all correspondence to Elliot Botvinick, Beckman Laser Institute, Department of Biomedical Engineering, 1002 Health Sciences Road East, Irvine, California 92612; Tel: (760) 845-6924; Fax: (858) 822-1160; E-mail: elliot.botvinick@uci.edu

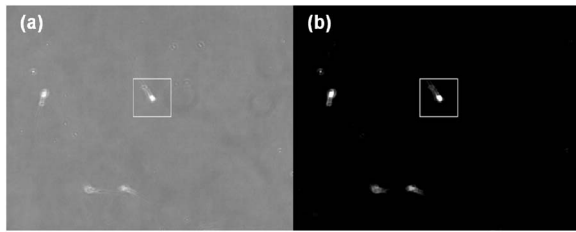


Fig. 1 (a) Raw phase contrast image of dog sperm acquired with a 40 \times oil immersion objective lens and a 0.33 \times demagnifier. Notice the contrast and brightness differences between the four sperm and the debris in the field, which are all at different focal positions relative to the high NA objective's focal plane. (b) Contrast enhancement produces a black background with bright sperm and debris. The square box indicates the ROI of the tracked sperm.

after trapping. Additionally, stable three-dimensional laser trapping requires a high numerical aperture (NA) oil immersion objective lens, which characteristically has very shallow depths of field (a few microns). As a result, swimming sperm routinely move in and out of focus as compared to imaging with a low NA air immersion objective lens. As a first attempt to automate tracking prior to and after trapping, video recorded during laser trapping experiments was played back into the HTM-IVOS CASA system (version 12.1, Hamilton Thorne Biosciences, 2004) equipped with an add-on feature for postvideo analysis and access to single sperm data. We found their algorithm failed to accurately report swimming parameters. Three error types that we noticed are (1) miscounting a single sperm as multiple sperm in a discontinuous path during transient focus change, (2) miscounting a single sperm as multiple sperm as two sperm paths intersect, and (3) cross-over events in which two sperm trajectories are swapped after their paths intersect. These errors are not mutually exclusive.

It became necessary to develop a more robust automated sperm tracking algorithm for single sperm trapping studies. A key design criterion was to transition the analysis away from offline postexperiment computation into a real-time video rate program with the goal of taking the joystick out of the hands of the experimenter. In previously published laser tweezers studies,^{8-10,12} the experimenter controlled the microscope stage via joystick to position a sperm-of-interest in the laser trap, a procedure that precluded experiments on fast swimming sperm. This paper describes a novel automatic sperm tracking algorithm called the single sperm tracking algorithm (SSTA), which solves the problems inherent in existing systems. A future publication will describe applying the algorithm in a video rate hands-free system for long-term tracking that culminates with computer-controlled trapping of the selected sperm, that is, "tack and trap."

2 Methods

2.1 Image Acquisition

The system setup and sperm preparation methods for laser trapping have been described in detail in Nascimento et al. (2006),¹² and Wang et al. (2005).¹³ A suspension¹² of 30 000 sperm per milliliter of Biggers, Whittens, and Whittingham (BWW) were loaded into a 2-mm deep cell culture chamber

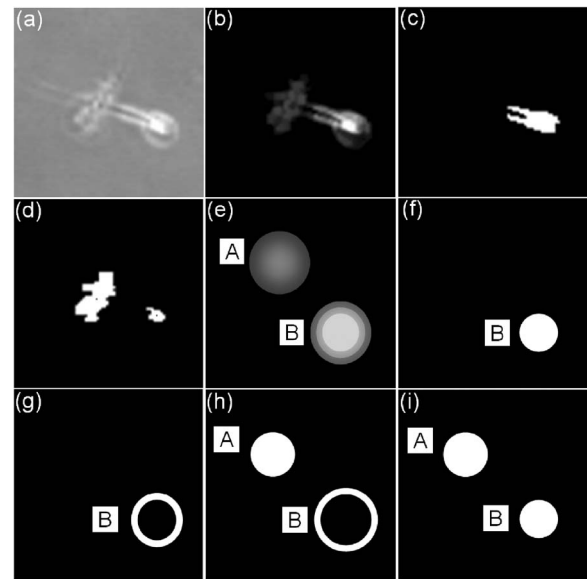


Fig. 2 (a) Raw phase contrast image containing two axially separated sperm; (b) after contrast enhancement; (c) binary mask demonstrates that two-class segmentation maps the dim sperm to the background; (d) binary mask demonstrates that SSTA's segmentation method finds both sperm. Gray pixels in the two white regions represent the calculated centroids; (e) for illustration, two phantom particles (particle A with low brightness and particle B with high brightness) represent the two sperm; (f) mask of the first (brightest) class contains the central portion of particle B; (g) the second class contains a portion of particle B; (h) the third class contains particle A and the dimmest pixels of particle B; (i) The final mask identifies pixels from both phantoms.

and placed on the microscope stage. The microscope stage was controlled by a joystick to locate and place a sperm-of-interest under the laser trap. A single sperm was held in the trap with either constant or decaying laser power. Prior to laser trapping, the microscope stage was momentarily halted (3 to 5 sec) to record video footage of the swimming sperm, after which the sperm was positioned in the laser trap. Similar footage was acquired after trapping. The frames of each video sequence were converted offline into bitmap format with ADOBE PREMIER PRO 1.5 (Adobe Systems Incorporated, San Jose, California).

2.2 Image Contrast Enhancement

SSTA was developed in the LABVIEW 7.1 language (National Instrument, Austin, Texas). SSTA loads and displays the first frame of a video sequence and a sperm-of-interest (i.e., the tracked sperm) is interactively selected with the computer's mouse. A square region of interest (ROI) is automatically created around the selected pixel as shown in Fig. 1. A background intensity was estimated, after calculation of the ROI's intensity histogram, as the sum of the most frequent intensity and the standard deviation. The background intensity was subtracted from each pixel in the ROI and the resulting image was linearly stretched to fill the intensity range (0 to 255), as shown in Fig. 1(b).

In order to continuously track a sperm with a high NA objective, it is essential to be able to extract the sperm from the background even when it appears slightly out of focus.

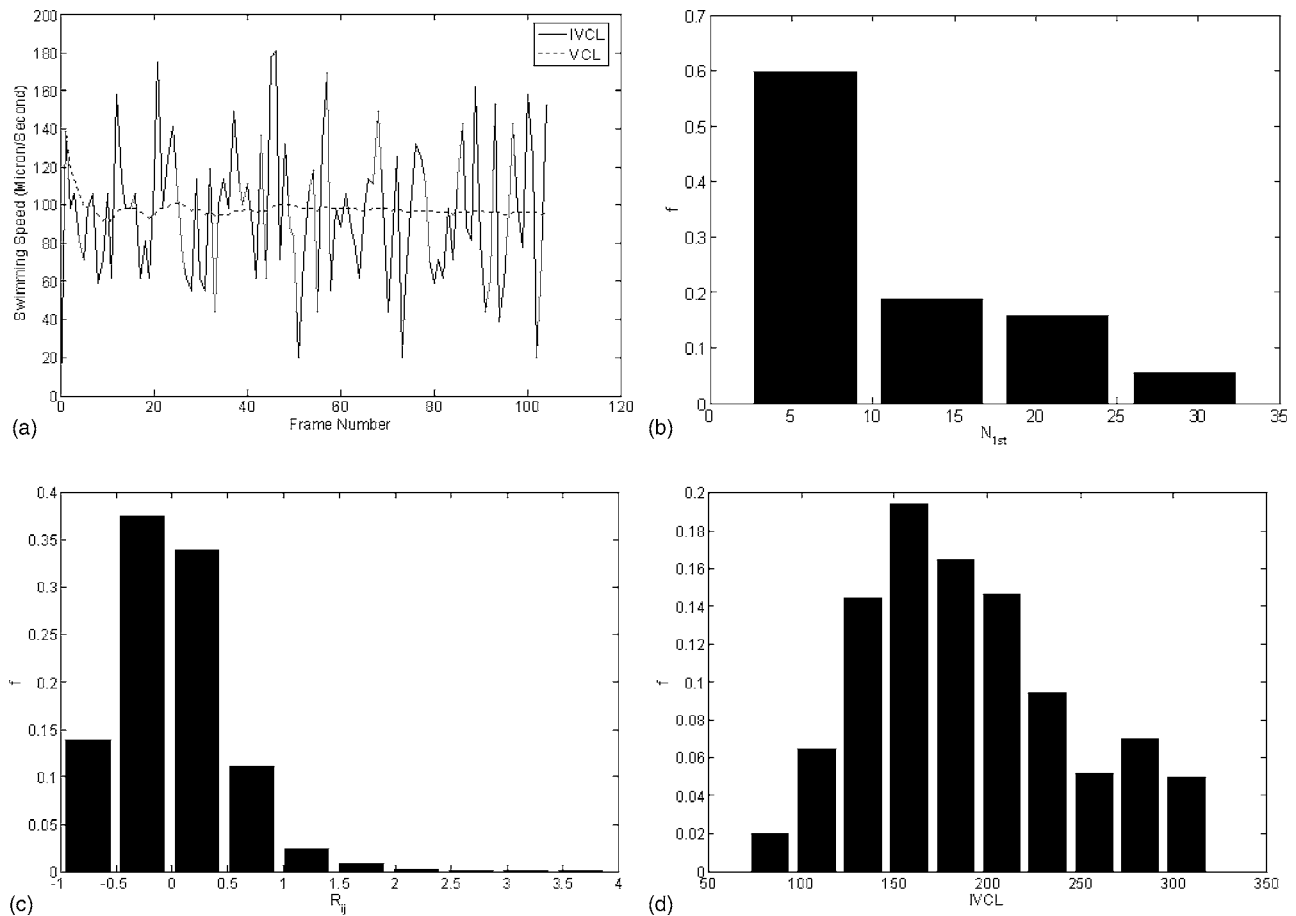


Fig. 3 Determination of speed-check parameters determined from the 200 noncollision sperm trajectories. (a) Plot of IVCL and VCL versus frame number for a randomly selected trajectory showing fluctuating IVCL and stabilizing VCL values; (b) distribution of N_{1st} shows more than half the occurrences fall in the first bin, or $N_{1st} < 10$; (c) distribution of $R_{i,j}$ (2 million observations), where $R_{i,j} = -1$ corresponds to $IVCL = 0$, and $R_{i,j} > 0$ corresponds to $IVCL > VCL$; (d) distribution of IVCL. Frequencies were normalized by the total number of observations.

Axial displacements on the order of a few microns will significantly change the focus quality and the contrast of the image.

2.3 Image Segmentation

SSTA uses custom image segmentation to create a binary image mask from each ROI to identify the sperm-of-interest. We found that the two-class thresholding algorithm was not suitable for tracking sperm in phase contrast. Tracked sperm may approach bright high contrast debris, nonmotile sperm, or other motile sperm within the ROI, as exemplified in Fig. 2(a). One sperm is clearly brighter than the second. Application of contrast enhancement [Fig. 2(b)] and a two-class thresholding dismisses the dim sperm as background [Fig. 2(c)]. Figure 2(e) used two phantom objects to represent the contrast enhanced image. The upper-left particle A represents an out-of-focus sperm-of-interest, while the lower-right particle B, represents an in-focus bright particle. Two-class thresholding dismisses A as background (not shown). SSTA calls the LABVIEW function IMAQ AutoMthreshold.vi, which implements an interactive clustering method seeking four pixel classes within the intensity histogram. Then the LABVIEW function IMAQ Threshold.vi is called once for each of the three brightest pixel classes to create a corresponding binary

mask [Figs. 2(f)–2(h)]. The first (and brightest) class contains the central bright region of particle B [Fig. 2(f)], while dimer pixels of B lie in the second and third classes [Figs. 2(g) and 2(h)]. The fourth class contains background pixels. Since B is represented in all three classes, it must be “merged” again into a single object. Binary dilation with a 3×3 structuring element is applied to the first class and projected onto the second class, setting the corresponding pixel value to zero. The process is repeated on the second class pixels and projected onto the third class. Resulting masks for the three classes are combined with a binary OR operator to calculate the final mask, which contains both particles as shown in Fig. 2(i). This method identifies both sperm in Fig. 2(a) as shown in Fig. 2(d). The LABVIEW function IMAQ Particle Analysis.vi measures the area, centroid (x, y) , and the bounding box for each particle. An area threshold of $10 \mu\text{m}^2$ was applied to remove small debris identified in the final mask.

2.4 Speed Check

We found that image segmentation alone could not consistently find the sperm-of-interest in the presence of other high-contrast objects. Speed check uses the curvilinear swimming speed (VCL) to further filter out interfering objects. SSTA uses the nearest neighbor method³ to associate objects in con-

secutive image frames. For those two frames, the instantaneous-VCL (IVCL) of an object is calculated as displacement divided by elapsed time. When image segmentation fails to identify the tracked sperm, IVCL will take on an uncharacteristic value as compared to VCL calculated over all previous frames. It was found that over time the VCL asymptotically stabilizes and variations in IVCL with respect to VCL are bound [Fig. 3(a)]. Let N_{min} be the minimum number of consecutive frames required to estimate the VCL within a defined range. Let R_{max} define the height of a window about VCL that bounds variations in IVCL. Let VCL_{max} be the species-dependent upper bound on IVCL. SSTA exploits these three physiologically derived bounds for its speed-check feature. That is, the most recently calculated IVCL is checked against two conditions

$$IVCL < R_{max} \times VCL \quad \text{if } N > N_{min}, \quad (1)$$

$$IVCL < VCL_{max} \quad \text{for all frames}, \quad (2)$$

where N is the current frame number and condition (2) acts as a ceiling condition (1).

N_{min} and R_{max} can be determined by analyzing a multitude of sperm swimming trajectories validated to contain no collisions or errors due to high contrast debris. We analyzed 200 such sperm trajectories. For each trajectory, let N_{1st} be the first frame after which the VCL of all subsequent frames is within 20% of the final VCL corresponding to that trajectory. The distribution of N_{1st} was examined over 200 trajectories to determine a suitable value for N_{min} [Fig. 3(b)]. Define $R_{i,j}$ as

$$R_{i,j} = \frac{IVCL_{i,j} - VCL_{f,j}}{VCL_{f,j}}, \quad (3)$$

where $IVCL_{i,j}$ is the swimming speed at the i 'th frame of the j 'th trajectory and $VCL_{f,j}$ is the final VCL of the j 'th trajectory. R_{max} can be determined by examining the distribution of $R_{i,j}$ across all 200 trajectories [Fig. 3(c)]. Similarly, VCL_{max} can be determined by examining the distribution of IVCL values across the sperm [Fig. 3(d)].

If either condition (1) or (2) fails, it is assumed that the detected particle in the current frame was erroneously identified. In the event that speed check detects a tracking error, pixel values within the bounding box (lengthened by 50%) of the incorrectly identified particle are replaced by the minimum intensity value of the ROI image. Image contrast enhancement and image segmentation are reapplied iteratively on the same frame until the conditions of speed check are satisfied or until all particles fail, in which case the next frame is acquired.

2.5 Collision Detection

As multiple sperm swim freely in the cell chamber, their paths often intersect. Collision detection is used to detect these events and to engage the algorithm of Sec. 2.6 to identify the correct sperm after intersection. In some cases, two sperm will collide resulting in a change of swimming direction, as illustrated in Fig. 4(a), while in other cases, axially separated sperm pass near each other only appearing to collide as demonstrated in Fig. 4(b). These were termed “real” and “per-

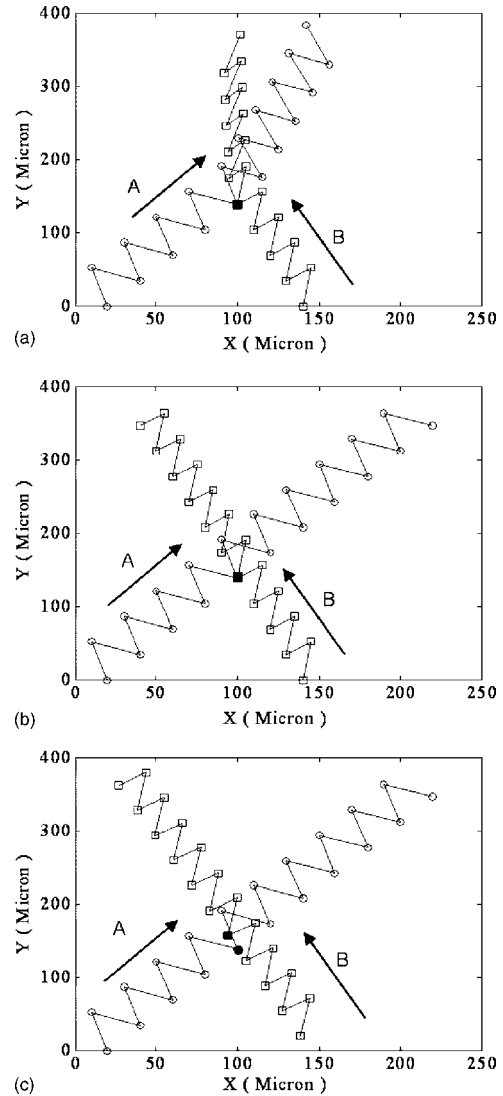


Fig. 4 Illustration of the three collision types defined in SSTA. The connected points represent centroid positions as sperm A (○) and sperm B (□) swim through the field. (a) In a real collision, two sperm physically collide resulting in changed swimming trajectories. Both sperm will be identified as the same object in at least one frame—in this example, frame 9 identified by the black square. (b) In a “perceived” collision, two sperm cross but remain axially separated. As with a real collision, both sperm will be identified as the same object in at least one frame—in this example, frame 9 identified by the black square. (c) In a “near-miss” collision, both sperm remain distinguishable, but a single sperm is the nearest neighbor to both sperm in the previous frame—in this example, sperm B in the ninth frame (■) is closer to sperm A and sperm B in the eighth frame and close still to sperm A in the ninth (●).

ceived” collisions, respectively.³ In the transverse image plane, two sperm may pass very close without colliding (remaining mutually distinguishable), as demonstrated in Fig. 4(c). This is termed a “near-miss.” SSTA regards near misses as collisions if a single sperm in one frame [i.e., the 9th point of B in Fig. 4(c)] is the nearest neighbor to both sperm in the previous frame [i.e., the 8th point of A and B in Fig. 4(c)]. SSTA employs collision detection to monitor for these three collisions. From the first frame where additional particles (in-

cluding sperm) are detected in the ROI, an additional ROI is created for each particle. The nearest neighbor method is then run in parallel for each particle within its ROI. The size of the ROIs were chosen such that, in accordance with Nyquist sampling theory, two sperm traveling directly toward each other at VCL_{max} would require at least two frames before they could collide, thus avoiding aliasing.

Let N_i be the first frame in which two sperm are detected in the ROI of the tracked sperm. Collision detection registers a collision if any of the following occurs:

1. Two sperm are no longer distinguishable in frame N_h , where $h > i$, and two distinguishable sperm with different centroid positions (X_j, Y_j) and (X'_j, Y'_j) are detected in frame N_j , where $j > h$ [i.e., Figs. 4(a) and 4(b); $h=9, j=10$].

2. Two sperm in frame N_{j-1} share the same nearest neighbor with centroid position (X_j, Y_j) in frame N_j , where $j > i$, while another sperm in frame N_j with a different centroid (X'_j, Y'_j) is closer to (X_j, Y_j) (i.e., Fig. 4(c); $j=9$).

2.6 Postcollision Analysis

Consider Fig. 5(a) where tracked sperm A swimming from point A_1 and second sperm B from point B_1 collide at point A_2 (coinciding with B_2). The two sperm separate along new trajectories toward points A_3 and B_3 , respectively. The purpose of postcollision analysis is to identify which of the new trajectories represent the precollision tracked sperm. Let N_c be the collision frame number and ΔN_c be the number of frames analyzed before and after N_c . A_1 and B_1 occur at $N_c - \Delta N_c$, while A_3 and B_3 occur at $N_c + \Delta N_c$. Net displacements are defined as L_{12} from A_1 to A_2 , L_{23A} from A_2 to A_3 , L_{23B} from A_2 to B_3 , L_{13A} from A_1 to A_3 , and L_{13B} from A_1 to B_3 , as shown in Fig. 5(b).

Three linearly independent criteria based on measurements of VCL (R_V), net displacement (R_D), and swimming angle (θ), were combined into a single cost function evaluated for each sperm such that the sperm with the greatest cost is identified as the correct sperm. To correctly calculate the VCL postcollision, ΔN_c was chosen to be twice the minimum frame number N_{min} . Collision-free trajectories were tracked to form distributions of the following two quantities:

1. $R'_{V_{i,j}}$, the ratio between VCL calculated from frame i to frame $(i + \Delta N_c)$, and VCL calculated from frame 1 to frame i (excluding ΔN_c points at each end) for each trajectory j

$$R'_{V_{i,j}} = \frac{\sum_{h=i}^{i+\Delta N_c} IVCL_{h,j}}{VCL_{i,j}}. \quad (4)$$

$R'_{V_{i,j}}$ measures the deviation of VCL calculated for frames i to $(i + \Delta N_c)$ with respect to VCL calculated on all previous i frames.

2. $R'_{D_{i,j}}$, the ratio between net sperm displacement observed over ΔN_c frames after and before frame i for trajectory j

$$R'_{D_{i,j}} = \frac{\sqrt{(x_{i+\Delta N_c,j} - x_{i,j})^2 + (y_{i+\Delta N_c,j} - y_{i,j})^2}}{\sqrt{(x_{i,j} - x_{i-\Delta N_c,j})^2 + (y_{i,j} - y_{i-\Delta N_c,j})^2}}. \quad (5)$$

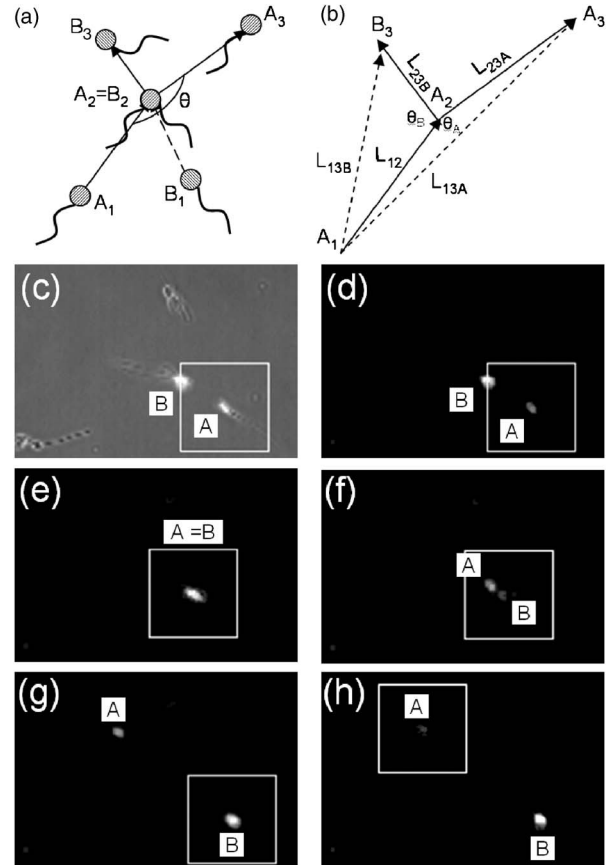


Fig. 5 Post collision analysis. (a) Illustration of a collision in which the tracked sperm starting at point A_1 and a second starting at point B_2 swim toward a common point $A_2=B_2$, collide, and swim in new trajectories toward A_3 and B_3 —it is unknown which sperm is the tracked one postcollision; (b) vector diagram measures displacements L and swimming angles θ between the precollision track of A and the two potential postcollision end points A_3 and B_3 ; (c) first frame in which a sperm B enters the ROI of tracked sperm A (raw phase contrast image); (d) enhanced image of (c); (e) first frame in which sperm A and sperm B merge (contrast enhanced); (f) first frame of separation is detected by collision detection and both sperm are tracked for 20 frames; (g) since sperm B in (f) is closest to the merged sperm in (e), the nearest neighbor method mistakenly identifies it as sperm A for the next 20 frames (notice the ROI is about sperm B); (h) postcollision analysis finds sperm A is 1000 times as likely as sperm B to be the correct sperm and the ROI is transferred to sperm A. Frame numbers: (c) (d)=29, (e)=34, (f)=40, (g)=59, (h)=60.

$R'_{V_{i,j}}$ or $R'_{D_{i,j}}$ will be unity whenever VCL or net sperm displacement are unaltered by the collision. SSTA transforms $R'_{V_{i,j}}$ and $R'_{D_{i,j}}$ through the Gaussian probability density function

$$f(z) = \exp\left\{-\frac{1}{2}[\alpha(z - z_0)]^2\right\}, \quad (6)$$

where z is $R'_{V_{i,j}}$ or $R'_{D_{i,j}}$, z_0 is unity, and the standard deviation $1/\alpha$ serves as a tunable parameter whereby the user can change the “steepness” of the transition from 1 to 0.

For a collision between sperm A and sperm B, let R_{V_k} ($k=A$ or B) be the VCL ratio and R_{D_k} be the net displacement ratio

$$R_{V_k} = \frac{VCL_k}{VCL_{N_c}}, \quad (7)$$

$$R_{Dk} = \frac{L_{23k}}{L_{12}} = \frac{\sqrt{(x_{k_3} - x_{A_2})^2 + (y_{k_3} - y_{A_2})^2}}{\sqrt{(x_{A_2} - x_{A_1})^2 + (y_{A_2} - y_{A_1})^2}}, \quad (8)$$

where VCL_k is the VCL from point k_2 to point k_3 [Figs. 5(a) and 5(b)], and VCL_{N_c} is the VCL of sperm A from frame 1 to frame N_c . Equation (6) is used to create two cost functions whereby variations observed in noncolliding sperm are used to rank the likelihood of variations observed following a collision.

$$C_{V_k} = \exp\left\{-\frac{1}{2}[\alpha_V(R_{V_k} - 1)]^2\right\}, \quad (9)$$

$$C_{Dk} = \exp\left\{-\frac{1}{2}[\alpha_D(R_{Dk} - 1)]^2\right\}, \quad (10)$$

where $1/\alpha_V$ and $1/\alpha_D$ are the standard deviations, which are tunable parameters used to adjust SSTA's sensitivity to variation.

The analysis of noncollision sperm trajectories does not provide information on sperm swimming angle (θ) following real collisions. Therefore the cost function for θ is not based on the noncollision sperm trajectories, but is chosen to favor small angle changes over large ones. The cost function is defined as

$$C_{\theta k} = \frac{1 - \cos \theta_k}{2}, \quad (11)$$

where

$$\cos \theta_k = \frac{L_{12}^2 + L_{23k}^2 - L_{13k}^2}{2L_{12}L_{23k}}, \quad (12)$$

and where $k=A$ or B . In Eq. (11), k increases monotonically from 0 to 1 as θ increases from 0 to 180 deg.

The three cost functions for sperm k are multiplied

$$C_k = C_{V_k}C_{\theta k}C_{Dk}, \quad (13)$$

and the sperm with the highest C_k is selected by SSTA as the correct sperm to continue tracking.

To compare SSTA to the popular commercial CASA system HTM-IVOS, identical image sequences must be analyzed. From 80 to 100 frames of video images, played back by a mini-digital video camcorder with a tape-time overlay, were captured by the HTM-IVOS system and analyzed. A HTM-IVOS add-on feature allows downloading of individual sperm trajectories within an analyzed image sequence. The same image frames were then selected for offline SSTA analysis. Trajectories were compared.

3 Results

Figure 3(a) plots IVCL and VCL for a sperm chosen at random from the 200 noncollision dog sperm trajectories. Figure 3(b) graphs the distribution of N_{1st} normalized by the number

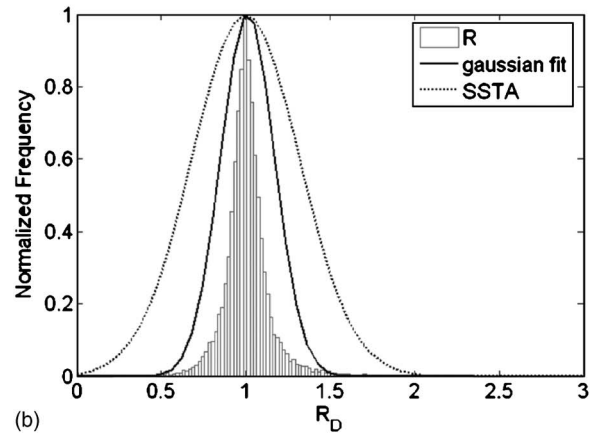
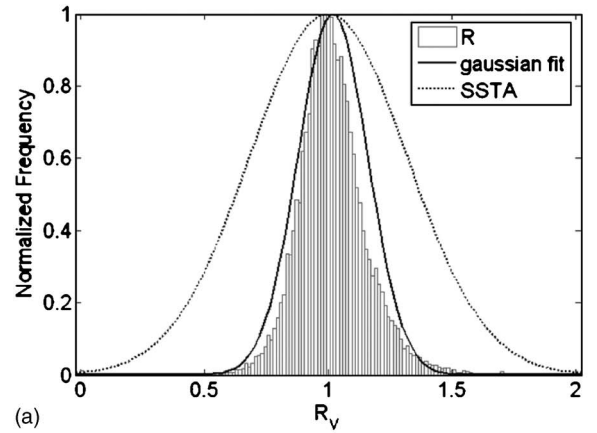


Fig. 6 (a) Distribution of $R'_{V_{ij}}$ (labeled R_V); (b) distribution of $R'_{D_{ij}}$ (labeled R_D). The distributions were first normalized such that integration under the curve yields unity and then scaled by their maximum frequency value in order to compare to Eqs. (9) and (10). (\square) are the normalized values, (—) the best Gaussian fit (—) and (---) Eq. (9) and (10) for (a) or (b), respectively, with $\alpha = \sqrt{10}$. Fit parameters for (a) are mean=1.0183 [1.0162, 1.003] and standard deviation=0.1401 [0.1387, 0.1416]; fit parameters for (b) are mean=1.0110 [1.0087, 1.0134] and standard deviation=0.1593 [0.1576, 0.1609] reported as value [95% confidence interval].

of observations. The 1st bin ($N_{1st} < 10$) contains 60% of the N_{1st} values. $N_{min}=10$ was selected for the speed-check feature.

Over two million values of R_{ij} were measured in the 200 trajectories. Figure 3(c) graphs the distribution of R_{ij} normalized by the number of observations. R_{ij} is mostly bound by $(-1, 3)$, where $R_{ij}=-1$ corresponds to $IVCL=0$, and $R_{ij}=3$ corresponds to $IVCL=4 \times VCL$. $R_{max}=4$ was selected for Eq. (1) of the speed-check feature.

Figure 3(d) graphs the distribution of IVCL normalized by the number of observations (over 950). The maximum observed IVCL=320 $\mu\text{m/s}$. VCL_{max} was set to 320 $\mu\text{m/s}$ in SSTA. Sperm swimming at VCL_{max} can travel 10.66 μm per frame and so the ROI dimension was set to $43.17 \times 43.17 \mu\text{m}$ (four times over sampling).

$R'_{V_{ij}}$ and $R'_{D_{ij}}$ were found to be unimodal and nonnormally distributed. Figure 6 shows their distributions with best-fit Gaussian curves as well as the corresponding SSTA equations

Table 1 Calculated parameters for the postcollision analysis of the video sequence represented in Fig. 5. The cost function C was orders of magnitude higher for sperm A, the correct sperm to track postcollision.

	Sperm B	Sperm A
VCL_k ($\mu\text{m/s}$)	65	83
VCL_{Nc} ($\mu\text{m/s}$)	NA	77
R_V	0.84	1.08
C_V	0.88	0.97
L_{23} (μm)	25.50	69.81
L_{12A} (μm)	NA	43.91
R_D	0.58	1.59
C_D	0.42	0.50
θ (deg)	4	172
C_θ	0.002	0.995
C	0.0006	0.49

[(9) and (10) $\alpha=100$]. The distributions were first properly normalized so that integration was unity and then scaled by their maximum frequency value in order to compare to Eqs. (9) and (10).

Figures 5(c)–5(h) shows selected frames taken before, during, and after a perceived collision event. The tracked sperm A swims from the lower-right to the upper-left corner of the field. Sperm A's ROI is indicated by the white box. A passing sperm B swims from the field's center to the lower-right corner entering the ROI in frame 29 [Fig. 5(c) raw image, 5(d) contrast enhanced]. Sperm A's and Sperm B's images overlap in frame 34 [Fig. 5(e)] with separation in frame 39 [Fig. 5(f)]. The nearest neighbor method mistakenly chose sperm B as sperm A since sperm B's centroid is nearer the overlapping sperm in the previous frame. For the next 20 frames, the ROI was assigned to sperm B [Fig. 5(g)]. Table 1 shows the collision cost function values for both sperm. Sperm A's score was higher by nearly 1000-fold, and sperm A was correctly selected for continued tracking as shown in frame 60 [Fig. 5(h)].

Table 2 compares key features used by SSTA and the HTM-IVOS for sperm tracking. Figures 7(a) and 7(b) show trajectories of two fluorescently labeled sperm (SYBR 14 dye) undergoing a near-miss collision. HTM-IVOS counted sperm 1 twice. SSTA correctly tracked both sperm, as validated by manual inspection. Table 3 lists VCL values for each track in Fig. 7. Differences in the two method's VCLs were 6.2 and 7.2% of the SSTA value for sperms 1 and 2, respectively. Figures 7(c) and 7(d) shows trajectories for another fluorescent image sequence with a near-miss collision type. Here the sperm-of-interest (sperm 3) crosses paths with a nearly

Table 2 Comparison of key features used by SSTA and the HTM-IVOS system for sperm tracking.

	HTM-IVOS	SSTA
Gray scale	256	256
Frame rate (Hz)	7–60	30
Consecutive frames	Up to 100	No limit
Search region	Circular of D_{\max}	Square $> 2 \times D_{\max}$
Sperm position	Brightness-weighted average position of head	Centroid of head
Collision	Not considered	Nearest neighbor, collision detection, postcollision analysis

orthogonally swimming sperm (sperm 4). HTM-IVOS terminated sperm 3's trajectory near the collision while merging sperm 4 and the continuation of sperm 3 into a single trajectory. SSTA was able to distinguish the two trajectories throughout the collision. As seen in Table 3, difference in VCL for sperms 5 and 6 were less than $\pm 5\%$ of the SSTA value.

Figures 8(a) and 8(b) show sperm trajectories from phase contrast images for the collision in Fig. 5. HTM-IVOS reported three sperm tracks: (1) sperm A prior to collision, (2) sperm B prior to collision merged with sperm A postcollision (labeled as A'), (3) sperm B postcollision (labeled as B'). SSTA correctly tracked both sperm, as validated by manual inspection. Figures 8(c) and 8(d) and Table 4 show trajectories for another phase contrast sequence. The nonintersecting sperm (sperms 7, 8, 9) have VCL differences as high as 22% of the SSTA values, with the SSTA's VCL values consistently higher. For the collision of sperms 10 and 11, the HTM-IVOS counted sperm 10 twice while SSTA tracked both sperm, again validated manually. There was a 19% difference in sperm 11's VCL.

4 Discussion

SSTA has been developed for use in laser trapping studies on sperm motility.¹² The algorithm was developed because the turnkey HTM-IVOS system committed frequent tracking errors as sperm swam out of focus. This is likely due to the high NA objective used in this study, which limits the depth of field to the scale of a sperm head. Consequently, even slight changes in axial position during swimming can significantly change the contrast of a sperm. The HTM-IVOS system is intelligently designed so that the chamber thickness matches the working distance of the objective lens and is therefore not sensitive to slight axial displacements of the sperm. It is reasonable that their algorithm struggled with the images in the laser trapping application. HTM-IVOS's inability to handle collision is well documented³ and was confirmed here. To address the focus issue, SSTA uses standard image contrast enhancement and custom four-class thresholding to extract

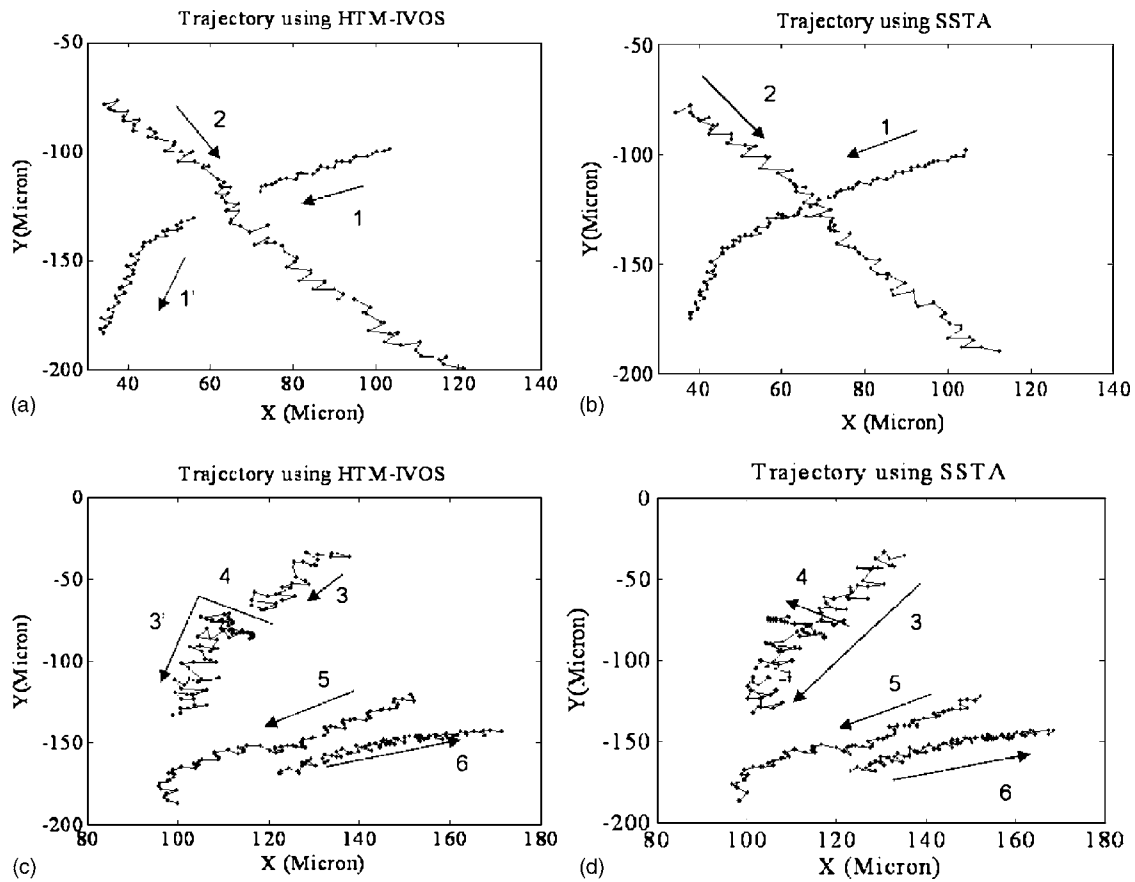


Fig. 7 Swimming trajectories from fluorescent image sequences containing collisions. (a) Trajectories analyzed by HTM-IVOS mistakenly severs sperm 1's trajectory into two (1 and 1') while assigning sperm 2 a continuous track, (b) SSTA analyses of the same sequence correctly reports the two continuous trajectories, (c) Trajectories analyzed by HTM-IVOS incorrectly merge sperm 4 with the postcollision segment of sperm 3 while correctly identifying sperm 5 and 6. The correct number of tracks is reported but a portion of sperm 3 is deleted while a new "hybrid" is created. (d) SSTA analyses of the same sequence and correctly separates sperm 4 and 3. Trajectories were verified manually.

sperm swimming with transient focus quality. SSTA's speed-check feature acts as a check on the thresholding method to find out-of-focus sperm swimming near high-contrast debris. To handle collisions, SSTA tracks all sperm in the ROI prior to and after a collision and uses its postcollision analysis to

statistically identify each sperm.

To train the system for collision events, SSTA analyzes noncolliding sperm trajectories to develop a statistical measure of normal deviations from mean swimming behaviors across multiple trajectories. From this analysis, SSTA con-

Table 3 VCLs and number of consecutive frames in the track for the six sperm represented in Fig. 7. Sperm labels correspond to labels in the figures. Results from the HTM-IVOS system and from SSTA are shown. The split rows for sperm 1 in the HTM-IVOS column represent the two tracks resulting from erroneous truncation of the single trajectory. The last column represents the percent difference in VCL values with respect to SSTA.

Algorithm	HTM-IVOS		SSTA		$\frac{(VCL_{HTM} - VCL_{SSTA})}{VCL_{SSTA}}$	
	Parameter	VCL ($\mu\text{m/s}$)	Frames	VCL ($\mu\text{m/s}$)		Frames
Sperm 1		54.7	25	53.4	80	6.2%
		58.7	40			
Sperm 2		98	80	91.4	80	7.2%
Sperm 3		106	31	116	80	-8.6%
Sperm 4		77	78	60	80	28%
Sperm 5		53.6	80	51	80	5%
Sperm 6		59.4	80	60	80	-1%

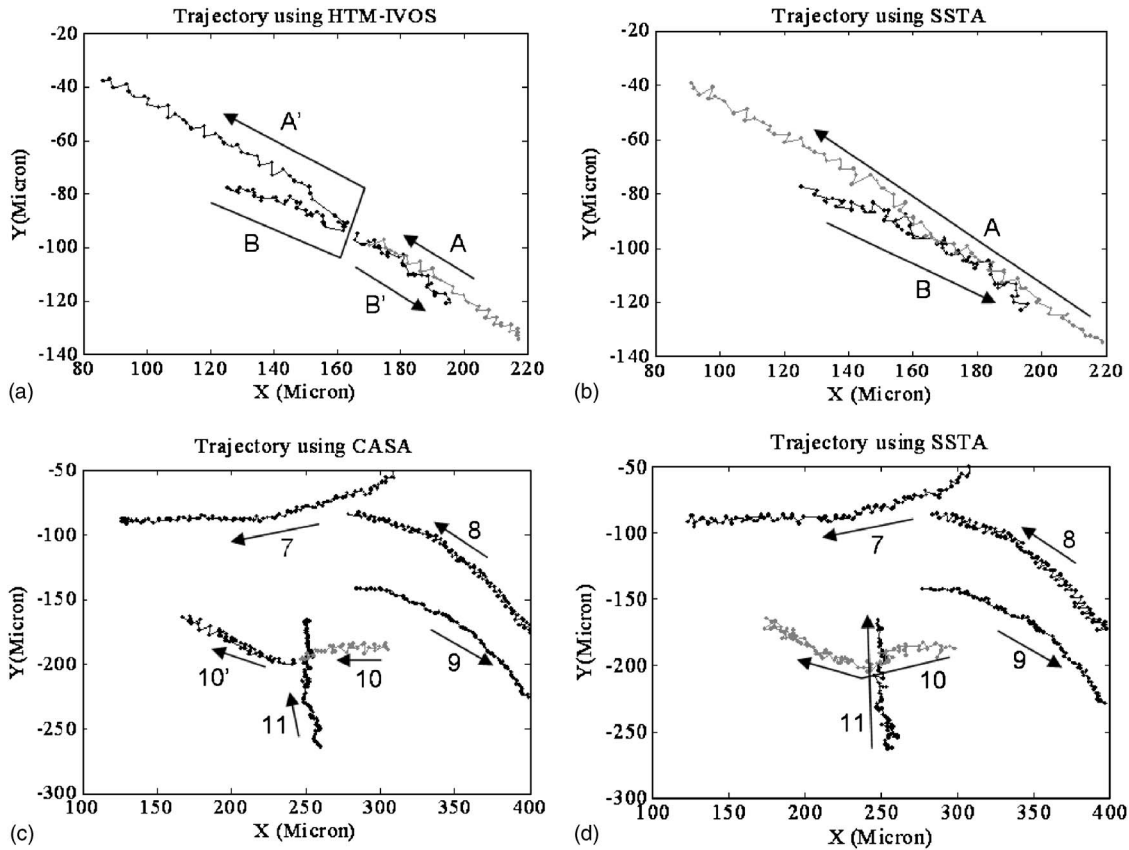


Fig. 8 Swimming trajectories from phase contrast image sequences containing collisions. (a) Trajectories analyzed by HTM-IVOS mistakenly merge sperm B with the postcollision segment of sperm A (A') while successfully tracking sperm A prior to collision and sperm B postcollision. (b) SSTA analyses of the same sequence and correctly reports the two continuous trajectories. (c) Trajectories analyzed by HTM-IVOS tracks three free swimming sperm (7, 8, 9), but mistakenly severs sperm 10 into two trajectories (10 and 10'), which were counted as separate sperm. SSTA analyzes and reports all five trajectories continuously. Note the increased lateral components of the SSTA tracks and compared to the HTM-IVOS tracks. Differences are likely due to SSTA seeking the binary mask centroid and HTM-IVOS seeking the brightness-weighted average to define the sperm's coordinates. Trajectories were verified manually.

structs costs functions to choose the most likely association before and after a collision based on the likelihood of pairing each precollision sperm with each postcollision sperm. SSTA allows the user to manually adjust the cost functions through

the α parameter, which changes the rate at which Eqs. (9) and (10) fall off toward zero as $R'_{V_{ij}}$ and $R'_{D_{ij}}$ depart from unity. The “naïve” samples of dog sperm tracked in Nascimento et

Table 4 VCLs and number of consecutive frames in the track for the five sperm represented in Figs. 8(c) and 8(d). Sperm labels correspond to labels in the figure. Results from the HTM-IVOS system and from SSTA are shown. The split rows for sperm 10 in the HTM-IVOS column represents the two tracks resulting from erroneous truncation of the single trajectory. The last column represents the percent difference in VCL values with respect to SSTA.

Algorithm	HTM-IVOS		SSTA		$\frac{(VCL_{HTM} - VCL_{SSTA})}{VCL_{SSTA}}$
	VCL ($\mu\text{m/s}$)	Frames	VCL ($\mu\text{m/s}$)	Frames	
Sperm 7	93.1	79	115	100	-19%
Sperm 8	107.5	80	115	100	-6.5%
Sperm 9	55.9	80	72	100	-22%
Sperm 10	105.5	28	119	100	-11%
	103.6	39			
Sperm 11	56.9	80	70	100	-19%

al.¹² were analyzed by SSTA using parameters obtained from the 200 trajectories described here.

Fluorescent images provide a “fair” test of SSTA tracking, in that the SYBR 14 dye produces bright nuclei with dark backgrounds making segmentation highly reliable. This allows a comparison of the SSTA’s tracking to that of the HTM-IVOS independent of the challenges of segmenting phase contrast images. For sperm swimming in noncolliding trajectories, there was only a $\pm 5\%$ difference in VCL as assessed by both systems (Table 3). This suggests that SSTA tracks well-defined objects in a similar way as the HTM-IVOS. However, sperm swimming in colliding trajectories had larger differences in VCL due to tracking errors in the commercial system. The advantage of SSTA for tracking single sperm is its ability to track colliding sperm, thereby avoiding miscounting or merging of trajectories. However, commercial CASA systems allow analysis of all sperm in the field even if collisions are mishandled.

Differences in VCL between SSTA and the HTM-IVOS when using phase contrast imaging are likely attributed to SSTA seeking the mask centroid and the HTM-IVOS seeking the brightness-weighted average to define the sperm center. While it is difficult to determine which is the correct method in the presence of blurring (caused as the sperm head rapidly moves from side to side), there is no justification in using brightness weighting because in phase contrast imaging the brightest pixels may not represent the geometrical center of the sperm head.

An algorithm based on the SSTA is being developed that can analyze all the sperm in the field and measure population statistics. While SSTA was developed to track a single sperm during laser trapping experiments (paper in press), it also offers an improved general method for tracking and measuring sperm.

Acknowledgments

We thank Dr. Barbara Durrant and her research group in the Arnold and Mabel Beckman Center for Conservation and Research of Endangered Species at the San Diego Wild Animal

Park for providing the dog sperm for our experiments. This work was supported by grants to MWB from the Air Force Office of Scientific Research (AFOSR Grant No. F9620-00-1-0371) and the National Institute of Health (Grant No. NIH RR 14892).

References

1. Y. Zhao, N. Vlahos, D. Wyncott, C. Petrella, J. Garcia, H. Zacur, and E. E. Wallach, “Impact of semen characteristics on the success of intrauterine insemination,” *J. Assist. Reprod. Genet.* **21**(5), 143–148 (2004).
2. R. P. Amann, and D. F. Katz, “Reflections on CASA after 25 years,” *J. Androl.* **25**(3), 317–325 (2004).
3. D. Mortimer, *Practical Laboratory Andrology* Oxford University Press, New York (1994).
4. J. S. Samuels and G. Van der Horst, “Sperm swimming velocity as evaluated by frame lapse videography and computer analysis,” *Arch. Androl.* **17**(2), 151–155 (1986).
5. D. T. Stephens, R. Hickman, and D. D. Hoskins, “Description, validation, and performance characteristics of a new computer-automated sperm motility analysis system,” *Biol. Reprod.* **38**(3), 577–586 (1988).
6. J. P. Le Pichon and J. C. Quero, “Microcomputer-based system for human sperm motility assessment and spermatozoon track analysis,” *Med. Biol. Eng. Comput.* **32**(4), 472–475 (1994).
7. W. Warchol, J. B. Warchol, K. Filipiak, Z. Karas, and F. Jaroszyk, “Analysis of spermatozoa movement using a video imaging technique,” *Histochem. Cell Biol.* **106**(5), 521–526 (1996).
8. M. J. Lang and S. M. Block, “LBOT-1: Laser-based optical tweezers,” *Am. J. Phys.* **71**(3), 201–215 (2003).
9. Y. Tadir, W. H. Wright, O. Vafa, T. Ord, R. H. Asch, and M. W. Berns, “Micromanipulation of sperm by a laser generated optical trap,” *Fertil. Steril.* **52**(5), 870–873 (1989).
10. K. Konig, L. Svaasand, Y. Liu, G. Sonek, P. Patrizio, Y. Tadir, and M. W. Berns, “Determination of motility forces of human spermatozoa using an 800 nm optical trap,” *Cell Mol. Biol. (Paris)* **42**(4), 501–509 (1996).
11. Z. N. Dantas, E. Araujo, Y. Tadir, M. W. Berns, M. J. Schell, and S. C. Stone, “Effect of freezing on the relative escape force of sperm as measured by a laser optical trap”
12. J. Nascimento, E. L. Botvinick, L. Z. Shi, B. Durrant, and M. W. Berns, “Analysis of sperm motility using optical tweezers,” *J. Biomed. Opt.* (2006) (in press).
13. Y. Wang, E. L. Botvinick, Y. Zhao, M. W. Berns, S. Usami, R. Y. Tsien, and S. Chien, “Visualizing the mechanical activation of Src.,” *Nature (London)* **434**(7036), 1040–1045 (2005).